

## LARGE EDDY SIMULATION OF MASS TRANSFER ACROSS AN AIR-WATER INTERFACE AT HIGH SCHMIDT NUMBERS

**Akihiko Mitsuishi, Yosuke Hasegawa, and Nobuhide Kasagi**

Department of Mechanical Engineering, The University of Tokyo,  
 Hongo 7-3-1, Bunkyo-ku, Tokyo 113-8656, JAPAN

E-mail: mituisi@thtlab.t.u-tokyo.ac.jp, hasegawa@thtlab.t.u-tokyo.ac.jp and kasagi@thtlab.t.u-tokyo.ac.jp

*Keywords: Mass Transfer, Turbulence, Air-Water Interface, High Schmidt Number, Large Eddy Simulation*

### ABSTRACT

Existing subgrid-scale (SGS) models for large eddy simulation are assessed for a problem of mass transfer across an air-water interface. A special focus is laid upon a case where the Schmidt number in the liquid phase ( $Sc_L$ ) is high. Dynamic Smagorinsky (DSM), dynamic mixed (DMM), and dynamic two-parameter (DTM) models are tested *a priori* at  $Sc_L = 1$  and 100 through comparisons with filtered direct numerical simulation (DNS) data.

For both  $Sc_L$  cases, the limiting behavior of Smagorinsky coefficient of the concentration field near the interface (see Fig. A1) is qualitatively well calculated by DSM. However, the serious underprediction causes poor estimation of the SGS stress and scalar flux. This is a serious issue in the high  $Sc_L$  case.

On the other hand, the scale-similarity type models, *i.e.*, DMM and DTM, keep good correlation with DNS (see Fig. A2) even at the high Schmidt number. The average SGS terms and SGS dissipation rates predicted by DTM are in better agreement with DNS than DMM. However, even the SGS terms calculated by DTM are not quantitatively accurate in the high  $Sc_L$  case.

It is concluded that, among the three models tested, DTM predicts the SGS contribution most accurately at high Schmidt numbers, although its quantitative predictability should still be improved.

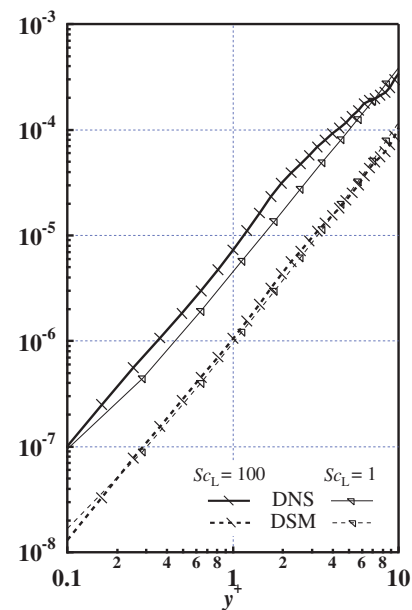


Fig. A1 Smagorinsky coefficient of concentration field in the liquid

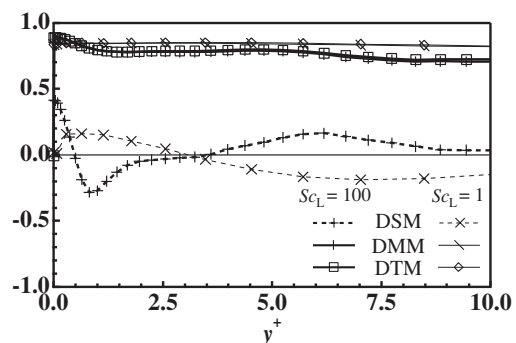


Fig. A2 Correlation coefficient of a vertical SGS flux of concentration field in the liquid

## NOMENCLATURE

- $C_s$  = Smagorinsky coefficient for velocity  
 $c$  = scalar concentration  
 $D_s$  = Smagorinsky coefficient for scalar concentration  
 $D_v$  = diffusion coefficient  
 $p$  = pressure  
 $Re$  = Reynolds number defined as  $u_\tau \delta / \nu$   
 $Sc$  = Schmidt number defined as  $\nu / D_v$   
 $S_{ij}$  = strain rate tensor  
 $u_i$  = velocity component in  $x_i$  direction  
 $u_\tau$  = interfacial friction velocity  
 $x_i$  = Cartesian coordinate system  
 $\bar{\Delta}$  = grid filter width  
 $\hat{\Delta}$  = test filter width  
 $\delta$  = half depth of computational volume  
 $\nu$  = kinematic viscosity  
 $\tau_{ij}$  = subgrid-scale stress tensor  
 $\xi_i$  = subgrid-scale scalar flux vector  
 $\langle \rangle$  = average in horizontal plane and time  
 $\bar{\phantom{x}}$  = grid-filtered value  
 $\hat{\phantom{x}}$  = test-filtered value

## INTRODUCTION

Detailed knowledge on mass transfer mechanism across a turbulent gas-liquid interface is of great importance to resolve the continuous global warming. Inaccurate estimation of dissolving greenhouse-effect gases such as  $\text{CO}_2$  from the atmosphere into the ocean directly leads to poor prediction of the future global climate change. This phenomenon is also important in industrial energy plants and chemical equipment.

Considering the fact that slightly soluble gases such as  $\text{CO}_2$  form a very thin concentration boundary layer in the liquid phase, detailed analysis of the flow and scalar concentration near the interface is strongly needed. To do this, a numerical approach is taken in the present work.

Direct numerical simulation (DNS) of free surface turbulence was first carried out by Lam and Banerjee [1], and followed by many researchers. More recently, Lombardi *et al.* [2] investigated the structures and statistics of a turbulent velocity field near a gas-liquid interface by means of DNS with an algorithm to solve each phase alternatively.

A defect of DNS is that its application is restricted to low Reynolds ( $Re$ ) and Schmidt ( $Sc$ ) numbers because of its high computational load, whereas the Reynolds number in most turbulent flows and the Schmidt number in  $\text{CO}_2$

absorption into the liquid are much more higher. This fact necessitates modeling of turbulence, *e.g.*, large eddy simulation (LES), which is capable of simulating unsteady flows with sufficient accuracy at reasonable computational cost.

An early concept of LES established by Smagorinsky [3] assumes that the stress from subgrid-scale is modeled by the turbulent eddy viscosity and the resolved local strain rate. Dynamic Smagorinsky model (DSM) proposed by Germano *et al.* [4] has notable improvement compared with the standard model and is widely used in LES calculations. In their procedure, the modeling coefficient is dynamically determined during computation.

On the other hand, by applying the dynamic procedure [4] to the mixed model of Bardina *et al.* [5], Zang *et al.* [6] proposed dynamic mixed model (DMM). More recently, Salvetti and Banerjee [7], by assuming a proportionality of the modified cross term to the modified Leonard term [8], proposed dynamic two-parameter model (DTM). They obtained better agreement with DNS than other dynamic models in *a priori* tests of free surface turbulence with no surface shear imposed.

Recently, Shen and Yue [9] made detailed research on LES of free surface turbulence, in which they visualized important structures such as the coherent vortices which play prominent roles in turbulent energy cascade, and they proposed a new model to reflect the anisotropic nature near the free surface.

Calmet and Magnaudet [10] carried out large eddy simulation of turbulent flow and scalar concentration field across an air-water interface at  $Sc_L = 200$ . However, detailed assessment of SGS models used was not been attempted.

The main objective of the present work is to assess ex-

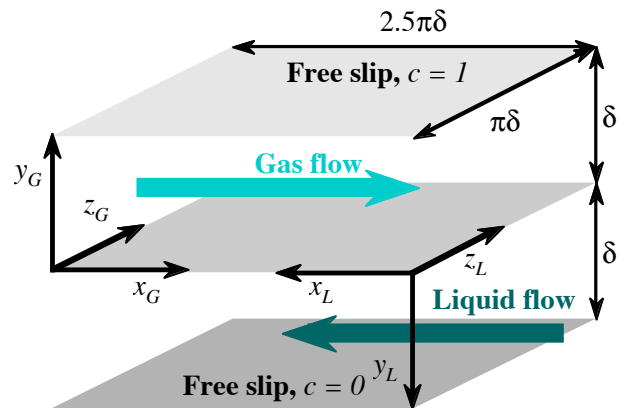


Fig. 1 Computational model of the coupled gas-liquid counter flow

isting SGS models and also to analyze the flow and concentration fields at high  $Sc$ . First, the SGS models described above are tested by using filtered DNS data for a case where  $Sc_L$  equals to 1. Then, the test is extended to a higher  $Sc_L$  (=100).

## COMPUTATIONAL CONDITIONS AND NUMERICAL METHOD

The computational volume is shown in Fig. 1. A gas-liquid counter flow across a flat interface is considered. The Reynolds number,  $Re$ , based on the interfacial friction velocity and the half depth of the whole computational volume is 150 in both gas and liquid phase. Since the effect of interface deformation on mass transfer is considered to be negligible at such a low  $Re$ , a flat interface is assumed in the calculation. The streamwise, vertical, and spanwise directions are denoted as  $x$  (or  $x_1$ ),  $y$  (or  $x_2$ ), and  $z$  (or  $x_3$ ), respectively. At each boundary, the following conditions are imposed:

- (a) gas-liquid interface
  - continuity of velocity and shear stress
  - Henry's law of scalar concentration
  - continuity of scalar flux
- (b) top and bottom planes of the computational volume
  - free-slip and constant concentration
- (c) other boundary planes (normal to  $x$  and  $z$  directions)
  - periodic boundary conditions

The pseudo-spectral method is employed with Fourier expansions in the  $x$  and  $z$  directions and Chebyshev expansion in the  $y$  direction. The algorithm to solve the coupled air and water phase is essentially the same as that of Lombardi *et al.*[2].

As is well known, LES needs spatial filtering to separate the unresolved subgrid-scale from the resolved grid-scale. In this paper, Gaussian filters are used in the statistically homogeneous (parallel to the interface) directions. Note that the filtering operation is done in the wave number space. A great advantage of this method is that data can be accurately filtered without interpolation.

The governing equations of LES of an incompressible flow and an associated scalar concentration field are given as follows:

$$\frac{\partial \bar{u}_i}{\partial x_i} = 0, \quad (1)$$

$$\frac{\partial \bar{u}_i}{\partial t} + \bar{u}_j \frac{\partial \bar{u}_i}{\partial x_j} = -\frac{\partial \bar{p}}{\partial x_i} + \frac{1}{Re} \frac{\partial^2 \bar{u}_i}{\partial x_j \partial x_j} - \frac{\partial \tau_{ij}}{\partial x_j}, \quad (2)$$

and

$$\frac{\partial \bar{c}}{\partial t} + \bar{u}_j \frac{\partial \bar{c}}{\partial x_j} = \frac{1}{Re \cdot Sc} \frac{\partial^2 \bar{c}}{\partial x_j \partial x_j} - \frac{\partial \xi_j}{\partial x_j}, \quad (3)$$

where all variables are normalized by the interfacial friction velocity,  $u_\tau$ , the half depth of the computational volume,  $\delta$ , the concentration difference between the top and the bottom of the volume,  $\Delta c$ , the kinematic viscosity,  $\nu$ , and the diffusion coefficient,  $D_\nu$ . The repeated indices follow Einstein's convention of summation. The last terms of the right-hand side of Eqs. (2) and (3) are related to the SGS stress and scalar flux, and they are modeled in terms of the resolved quantities and defined as follows:

$$\tau_{ij} = \overline{u_i u_j} - \bar{u}_i \bar{u}_j \quad (4)$$

and

$$\xi_i = \overline{c u_i} - \bar{c} \bar{u}_i. \quad (5)$$

The grid- and test-filtered strain rate tensor and the related term are defined below:

$$\bar{S}_{ij} \equiv \frac{1}{2} \left( \frac{\partial \bar{u}_i}{\partial x_j} + \frac{\partial \bar{u}_j}{\partial x_i} \right), \quad (6)$$

$$|\bar{S}| \equiv (2 \bar{S}_{ij} \bar{S}_{ij})^{1/2}, \quad (7)$$

$$\hat{S}_{ij} \equiv \frac{1}{2} \left( \frac{\partial \hat{u}_i}{\partial x_j} + \frac{\partial \hat{u}_j}{\partial x_i} \right), \quad (8)$$

and

$$|\hat{S}| \equiv (2 \hat{S}_{ij} \hat{S}_{ij})^{1/2}. \quad (9)$$

Three models tested are summarized below. Their modeling coefficients are calculated by taking the least square error minimization technique [11] to the Germano's identity [4] for Eqs. (10) - (15) in each horizontal plane.

### Dynamic Smagorinsky Model (DSM)

$$\tau_{ij} - \frac{1}{3} \tau_{kk} \delta_{ij} = -2 C_s \bar{\Delta}^2 |\bar{S}| \bar{S}_{ij} \quad (10)$$

$$\xi_i = -D_s \bar{\Delta}^2 |\bar{S}| \frac{\partial \bar{c}}{\partial x_i} \quad (11)$$

### Dynamic Mixed Model (DMM)

$$\tau_{ij} = (\overline{\bar{u}_i \bar{u}_j} - \bar{u}_i \bar{u}_j) + C_s (-2 \bar{\Delta}^2 |\bar{S}| \bar{S}_{ij}) \quad (12)$$

$$\xi_i = (\overline{\bar{c} \bar{u}_i} - \bar{c} \bar{u}_i) + D_s \left( -\bar{\Delta}^2 |\bar{S}| \frac{\partial \bar{c}}{\partial x_i} \right) \quad (13)$$

### Dynamic Two-parameter Model (DTM)

$$\tau_{ij} = C_B (\overline{\bar{u}_i \bar{u}_j} - \bar{u}_i \bar{u}_j) + C_s (-2 \bar{\Delta}^2 |\bar{S}| \bar{S}_{ij}) \quad (14)$$

$$\xi_i = D_B (\overline{\bar{c} \bar{u}_i} - \bar{c} \bar{u}_i) + D_s \left( -\bar{\Delta}^2 |\bar{S}| \frac{\partial \bar{c}}{\partial x_i} \right) \quad (15)$$

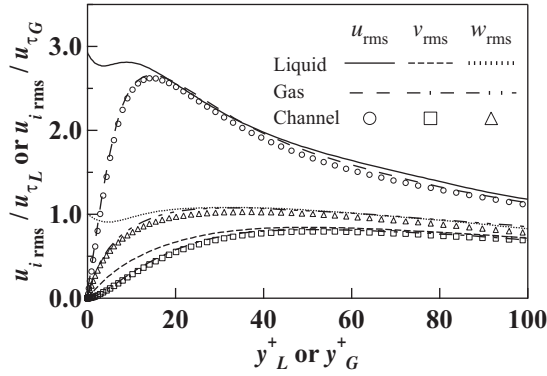


Fig. 2 Velocity intensities of each phase

### CHARACTERISTICS OF FLOW AND SCALAR FIELDS

In this chapter, the results of DNS of a coupled air-water flow are shown to summarize the characteristics of both the flow and scalar field.

The velocity fluctuations in the two phases are shown in Fig. 2. The profiles in the two phases are similar to those of a channel flow far from the interface, while large differences arise near the interface. Note that all these values are non-dimensionalized by the interfacial friction velocity  $u_{\tau G}$  or  $u_{\tau L}$  of each phase. In the gas phase, the velocity fluctuations decrease as the interface is approached and show good agreement with those near a no-slip wall. On the other hand, the streamwise and spanwise velocity fluctuations show the maximum values at the interface of the liquid phase.

These differences result from the large density ratio of the two phases. The interface works as a no-slip boundary for the gas phase, while as a free-surface for the liquid phase.

The mean scalar concentration profile at  $Sc_G = Sc_L = 1$  is shown in Fig. 3. Although the Schmidt numbers in both phases are the same, most mass transfer resistance occurs in the liquid phase. In Fig. 4, the root-mean-square (rms) value of scalar fluctuations, normalized by interfacial friction concentration, *i.e.*,  $1/u_{\tau} \cdot D_v \partial \bar{c} / \partial y|_{interface}$ , of both phases are shown. The interface seems to impose a constant scalar concentration boundary condition in the liquid phase, while allows the maximum scalar fluctuation in the gas phase.

### RESULTS OF A PRIORI TESTS AT $Sc_L = 1$

Each SGS model (DSM, DMM, and DTM) is tested *a priori* in predicting the SGS stresses and scalar fluxes. The spatially filtered DNS data of flow and concentration fields is used. The statistics are averaged in the horizontal plane

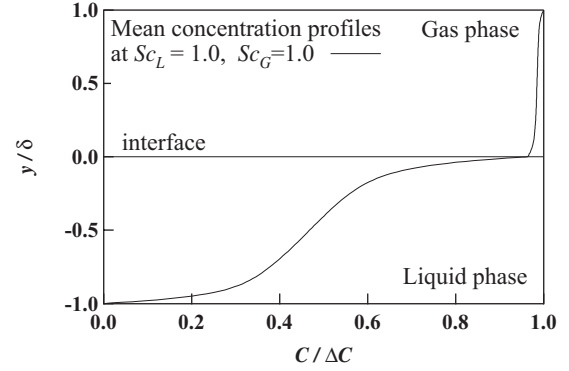


Fig. 3 Mean scalar concentration of both phases

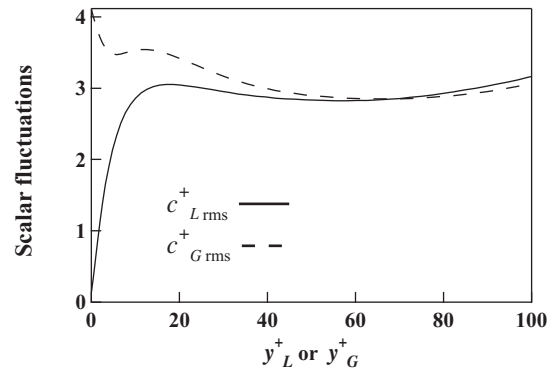


Fig. 4 Scalar fluctuations of each phase

and given as functions of the distance from the interface. For DNS calculation, 64 Fourier modes in both streamwise and spanwise ( $x$  and  $z$ ) directions and 48 Chebyshev polynomials in the vertical ( $y$ ) direction are employed. As is mentioned in the computational conditions, the Gaussian filters in  $x$  and  $z$  directions are applied for the SGS models. The widths of the grid and the test filter are defined as:

$$\bar{\Delta} = (\bar{\Delta}_x \bar{\Delta}_z)^{1/2} \quad \text{and} \quad \hat{\Delta} = (\hat{\Delta}_x \hat{\Delta}_z)^{1/2}. \quad (16)$$

Presently, the grid filter width is four times the grid spacing of DNS, while the test filter width is twice that of the grid filter.

First, the model coefficients of the Smagorinsky part,  $C_s$  and  $D_s$ , of each model are shown in Figs. 6 and 7. Here, the line denoted as ‘optimal’ is the plane-optimized value and obtained by applying the least square technique directly to Eq. (10) (or Eq. (11)), not to the Germano’s identity, in each horizontal plane. In Fig. 6, distinctions of  $C_s$  and  $D_s$  of each phase become significant near the interface. The coefficients, determined by the relations of  $\tau_{ij}$  (or  $\xi_r$ ) and  $\bar{S}_{ij}$  (or  $\partial \bar{c} / \partial x_i$ ), of the gas side and the liquid side behave dif-

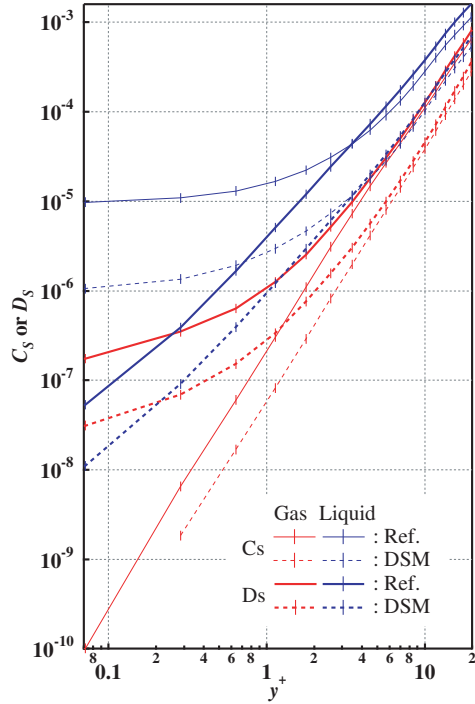


Fig. 6 Plane-averaged  $C_s$  or  $D_s$  in each phase

ferently from each other as they come close to the interface. Considering the final goal, *i.e.*, to model the concentration field at higher  $Sc_L$ , SGS model must express such characteristics of the coefficients in the liquid. Although its absolute value is underestimated, the dynamic procedure predicts qualitatively well the mass transfer near the interface. Hereafter, we focus on the liquid phase, because the gas phase transfer near the interface is similar to that near the solid wall.

Figures 7 (a) and (b) show plane-optimized and modeled  $C_s$  and  $D_s$  in the liquid phase. In general, the values of  $C_s$  and  $D_s$  are largest in DSM, followed by DMM and DTM, which produce most of their SGS contributions by the scale similarity terms.

In Figs. 8 (a), (b), and (c), the plane-averaged  $\tau_{11}$ ,  $\tau_{12}$ , and  $\xi_2$  computed by DSM, DMM, and DTM, calculated with the filtered DNS data using the Eqs. (10) - (15), are compared with DNS. It is seen that DMM and DTM reproduce the DNS data much better than DSM. DSM completely fails in modeling  $\tau_{11}$ , because DSM does not account for the modified Leonard and cross terms [7]. In addition, DTM shows slightly better agreement with DNS than DMM. However, the underestimation of these quantities is not negligible even in DTM. The peak value of the SGS scalar flux in DTM is almost two thirds of the DNS data. The similar tendency is also observed in other com-

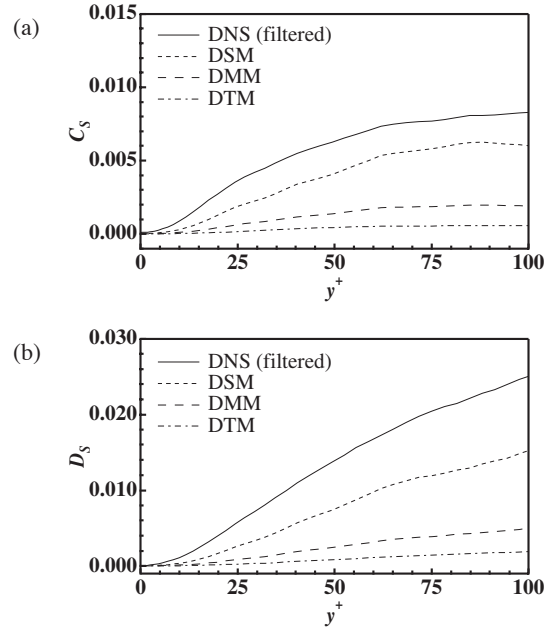


Fig. 7 (a);  $C_s$  and (b);  $D_s$  of each model

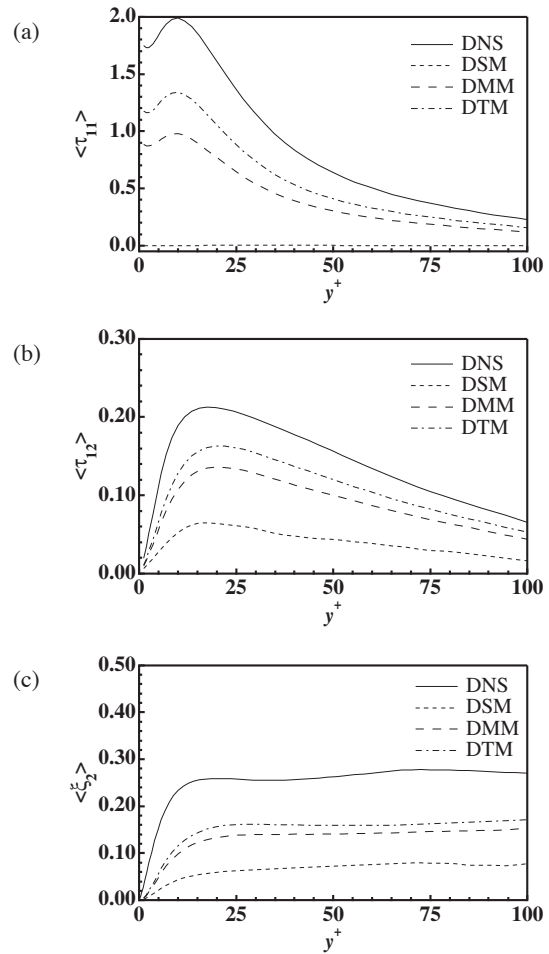


Fig. 8 Plane-averaged SGS terms (a);  $\langle \tau_{11} \rangle$ , (b);  $\langle \tau_{12} \rangle$ , and (c);  $\langle \xi_2 \rangle$

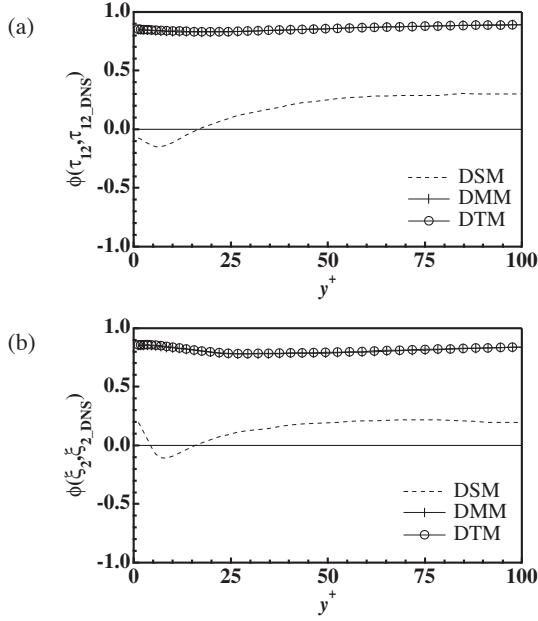


Fig. 9 Correlation coefficient of (a);  $\tau_{12}$  and (b);  $\xi_2$

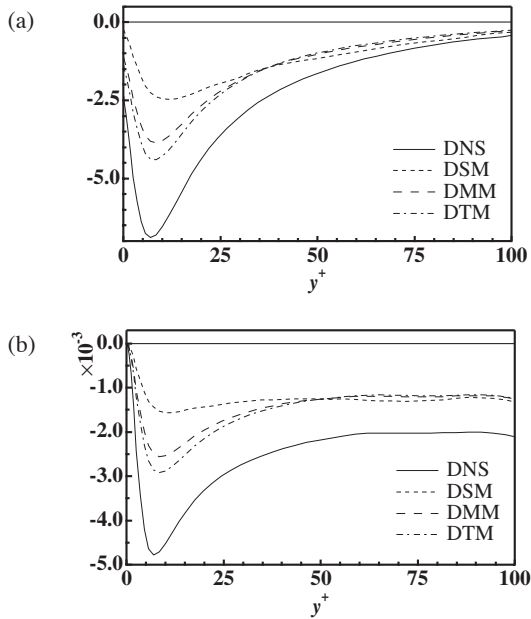


Fig. 10 Plane-averaged SGS dissipation rate  
(a);  $\langle \tau_{ij} \bar{S}_{ij} \rangle$  and (b);  $\langle \xi_i \cdot \partial \bar{c} / \partial x_i \rangle$

ponents of the SGS stress and scalar flux.

In order to evaluate the fluctuation around the mean value of the SGS stress and scalar flux, correlation coefficients between the exact and modeled SGS terms are calculated. The correlation coefficient between two variables,  $a$  and  $b$ , is defined as

$$\phi(a, b) \equiv \frac{\langle ab \rangle - \langle a \rangle \langle b \rangle}{\left\{ \left( \langle a^2 \rangle - \langle a \rangle^2 \right) \left( \langle b^2 \rangle - \langle b \rangle^2 \right) \right\}^{1/2}}. \quad (17)$$

Figures 9 (a) and (b) show vertical profiles of the correlation coefficients of  $\tau_{12}$  and  $\xi_2$ , respectively. It is evident that DMM and DTM perform much better than DSM and result in a very high correlation coefficient (0.8 ~ 0.9) with DNS. These results are in good agreement with previous studies (e.g. [7]) on open channel flows.

The SGS dissipation rates,  $\tau_{ij} \bar{S}_{ij}$  for the velocity and  $\xi_i \cdot \partial \bar{c} / \partial x_i$  for the scalar concentration, are shown in Figs. 10 (a) and (b). These values are the rates of energy transfer from grid- to subgrid-scales. DTM shows the best agreement with DNS near the interface. As is discussed in Fig. 8, the absolute energy transfer from the grid to the subgrid scales is not sufficient in all models tested. Among the three models, however, DTM gives the best result.

#### RESULTS OF A PRIORI TESTS AT $Sc_L = 100$

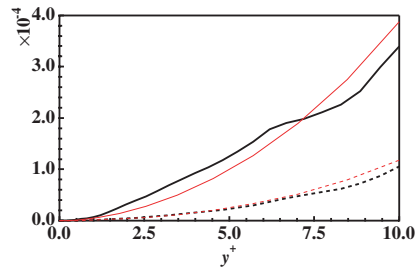
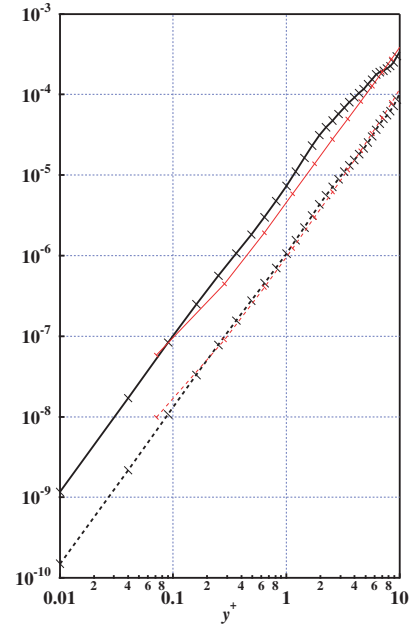


Fig. 11.  $D_s$

$Sc_L = 100$        $Sc_L = 1$   
 — DNS      — DMM  
 - - - DSM      - - - DTM

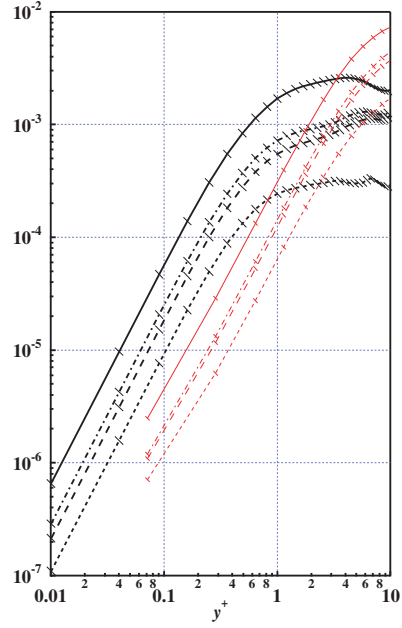


Fig. 12. Plane-averaged  $\xi_2$

$Sc_L = 100$	$Sc_L = 1$
— DNS	— DNS
- - - DSM	- - - DSM
- · - DMM	- · - DMM
· · · DTM	· · · DTM

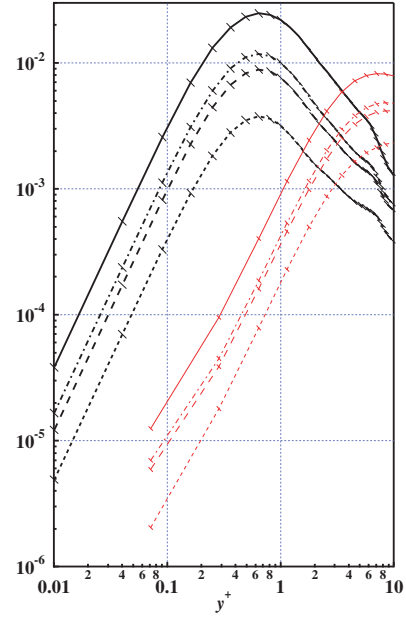
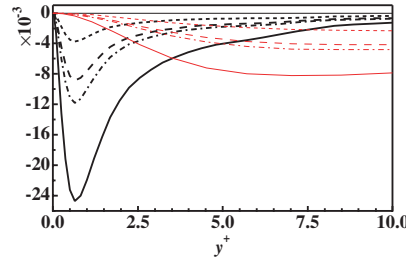
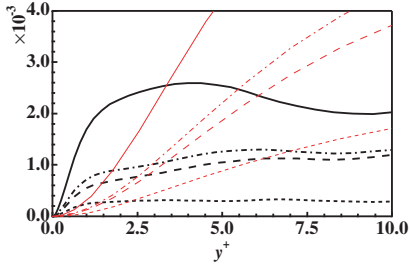


Fig. 14. Plane-averaged SGS dissipation rate

$Sc_L = 100$	$Sc_L = 1$
— DNS	— DNS
- - - DSM	- - - DSM
- · - DMM	- · - DMM
· · · DTM	· · · DTM



*A priori* tests are extended to the case of  $Sc_L = 100$ . In order to resolve the fine scale scalar fluctuations in a thin concentration boundary layer at this high Schmidt number, the computational grid in the liquid is shrunk toward the

interface, and the scalar field near the interface ( $0 \leq y^+ \leq 20$ ) is calculated by applying a finite difference method in the vertical direction. The concentration field of the liquid phase is resolved with 192 Fourier modes in the streamwise and spanwise ( $x$  and  $z$ ) directions and 48 grid points in the vertical ( $y$ ) direction.

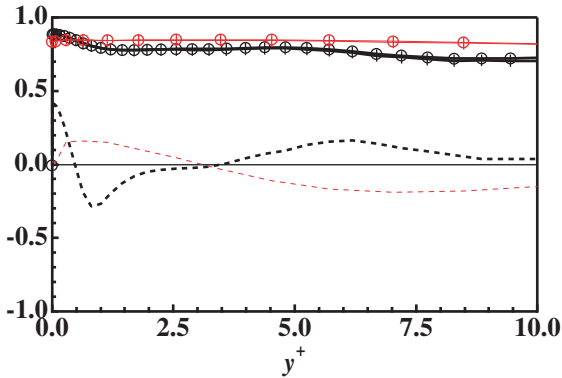


Fig. 13. Correlation coefficient of  $\xi_2$

$Sc_L = 100$	$Sc_L = 1$
- - - DSM	- - - DSM
- · - DMM	- · - DMM
· · · DTM	· · · DTM

The coefficient of  $D_s$  computed by DSM is shown in Fig. 11, together with the plane-optimized value. It should be emphasized that the limiting behavior of the plane-optimized Smagorinsky coefficients only weakly depends on  $Sc$ . Again, DSM can give qualitatively accurate coefficients, but underestimates their values considerably.

As a typical sample of the plane-averaged SGS terms, the vertical component,  $\xi_2$ , is shown in Fig. 12. It is found from the limiting behavior near the interface that all the dynamic models can qualitatively capture the characteristics of the DNS data. DTM shows again particularly the best agreement with DNS as in the low  $Sc_L$  case.

The correlation coefficients of the exact and predicted  $\xi_2$  are shown in Fig. 13. Despite of a large difference in  $Sc$ , DTM and DMM show very good correlation with the DNS results indicating that the models of scale-similarity type keep their accuracy in modeling the local SGS scalar flux even at higher  $Sc$ .

Figure 14 shows the SGS dissipation rate. The tendency similar to the low  $Sc_L$  case is observed. Although the absolute values predicted are not sufficiently accurate, DTM gives the best result among the three models.

### CONCLUDING REMARKS

*A priori* tests of existing subgrid-scale models for LES were carried out on mass transfer across an air-water interface at Schmidt numbers of  $Sc = 1$  and 100. For both cases, DTM shows the best results among the tested three models.

To obtain guidelines for modeling, we overviewed the characteristics of each phase in the air-water counter flow by examining the DNS data in the case of  $Sc_L = 1$ . The asymptotic behavior of plane-optimized  $C_s$  and  $D_s$  clarify the necessity of accurate modeling of the SGS terms, especially close to the interface in the liquid phase.

For the same case, three dynamic SGS models were tested *a priori*. For both flow and concentration field, the plane-averaged SGS terms are modeled by DTM better than DMM and DSM. The correlation coefficients of  $\tau_{12}$  and  $\xi_2$  given by DTM and DMM with DNS are much higher than those by DSM. The SGS dissipation rates modeled by DTM are better than those by DSM and DMM especially near the interface.

At a higher Schmidt number ( $Sc_L = 100$ ), the plane-optimized Smagorinsky coefficients are found to be almost independent of the Schmidt number. This fact suggests validity of employing models of the eddy diffusivity type with the constant turbulent Schmidt number in a wide range of the Schmidt number. However, DSM fails to predict the local SGS scalar flux at both high and low Schmidt numbers. On the other hand, DTM can capture the local SGS flux quite accurately even at a higher Schmidt number.

These findings indicate superiority of DTM in mass transfer across an air-water interface at high Schmidt numbers.

### REFERENCES

- [1] Lam, K., and Banerjee, S., "On the condition of streak formation in a bounded turbulent flow," *Phys. Fluids, A* **4** (2), pp. 306-320.
- [2] Lombardi, P., De Angelis, V., and Banerjee, S., "Direct numerical simulation of near-interface turbulence in coupled gas-liquid flow," *Phys. Fluids*, **8** (6) (1996), pp. 1643-1665.
- [3] Smagorinsky, J., "General circulation experiments with the primitive equations," *Mon. Weather Rev.*, **93**, 1963, pp. 99-164.
- [4] Germano, M., Piomelli, U., Moin, P., and Cabot, W. H., "A dynamic subgrid-scale eddy viscosity model," *Phys. Fluids, A* **3** (7), 1991, pp. 1760-1765.
- [5] Bardina, J., Ferziger, J. H. and Reynolds, W. C., "Improved turbulence models based on large eddy simulation of homogeneous, incompressible turbulent flows," *Dept. Mech. Engng., Stanford Univ. Rep.*, 1984, TF-19.
- [6] Zang, Y., Street, R. L. and Koseff, J. R., "A dynamic mixed subgrid-scale model and its application to turbulent recirculating flows," *Phys. Fluids, A* **5** (12), 1993, pp. 3186-3196.
- [7] Salvetti, M. V. and Banerjee, S., "*A priori* tests of a new subgrid-scale model for finite-difference large-eddy simulations," *Phys. Fluids*, **7** (11), 1995, pp. 2831-2847.
- [8] Germano, M., "A proposal for a redefinition of the turbulent stresses in the filtered Navier-Stokes equations," *Phys. Fluids*, **29** (7), 1986, pp. 2323-2324
- [9] Shen, L. and Yue, D. K. P., "Large-eddy simulation of free-surface turbulence," *J. Fluid Mech.*, **440**, 2001, pp. 75-116.
- [10] Calmet, I. and Magnaudet, J., "High-Schmidt number mass transfer through turbulent gas-liquid interfaces," *Int. J. Heat and Fluid Flow*, **19**, 1998, pp. 522-532.
- [11] Lilly, D. K., "A proposed modification of the Germano subgrid-scale closure method," *Phys. Fluids, A* **4** (3), 1992, pp. 633-635.